

# Characterization of the Physical State of Spray-Dried Inulin

Sébastien N. Ronkart · Claude Deroanne ·  
Michel Paquot · Christian Fougnes ·  
Jean-Christophe Lambrechts · Christophe S. Blecker

Published online: 20 July 2007  
© Springer Science + Business Media, LLC 2007

**Abstract** Modulated differential scanning calorimetry, wide angle x-ray scattering, and environmental scanning electron microscopy were used to investigate the physical and morphological properties of chicory root inulin spray dried under different conditions. When the feed temperature increased up to 80 °C, the average degree of polymerization of the solubilized fraction increased, leading to a higher glass transition temperature (T<sub>g</sub>). Above 80 °C, the samples were completely amorphous, and the T<sub>g</sub> did not change. The starting material was semicrystalline, and the melting region was composed of a dual endotherm; the first peak subsided as the feed temperature increased up to a temperature of 70 °C, whereas above 80 °C, no melting peak was observed as the samples were completely amorphous. To a lesser extent, the inlet air temperature of 230 °C allowed a higher amorphous content of the samples than at 120–170 °C but induced a blow-out of the particles.

**Keywords** Inulin · Spray drying · Glass transition · MDSC · WAXS · ESEM

## Introduction

Inulin is a natural storage carbohydrate mainly found in plants from the *Asteraceae* family. It is not a simple molecule but a mixture of oligo- and/or polysaccharides composed of fructose unit chains (linked by  $\beta$ -D-(2 $\rightarrow$ 1) D-fructosyl-fructose bonds) of various length, terminated generally by a single glucose unit (linked by an  $\alpha$ -D-glucopyranosyl bond).<sup>1</sup> The use of inulin and derivatives in the food industry is in constant increase, and the main benefits and nutritional interests of these products are broadly discussed in the literature.<sup>2,3</sup> For now, commercial inulin is extracted from chicory root and is available as a spray-dried powder product, which has the advantage of low production costs compared to other drying techniques (e.g., freeze drying). Spray-drying produces particles by atomizing a solution or slurry (named feed) and evaporating moisture from the resulting droplets by suspending them in a hot gas.<sup>4</sup> Whereas moving in this hot medium, the droplets are dried into individual or agglomerate powder particles. In the industry, the spray-drying technology is usually only considered as an evaporating technique; the main reason is probably that spray-drying trials remain very complicated and expensive under industrial conditions. For this reason, pilot scale spray driers are interesting tools for investigating the influence of feed characteristics or drying parameters on the physical properties of the powder.

Previous studies on spray drying of carbohydrates have paid a great attention to the effects of the operational conditions of the drier, but very few authors have discussed the importance of the feed characteristics. This aspect of spray drying is important because the nature of the spray-dried

---

S. N. Ronkart (✉) · C. Deroanne · C. S. Blecker  
Department of Food Technology,  
Gembloux Agricultural University,  
Passage des Déportés, 2,  
5030 Gembloux, Belgium  
e-mail: ronkart.s@fsagx.ac.be

S. N. Ronkart · M. Paquot  
Department of Industrial Biological Chemistry,  
Gembloux Agricultural University,  
Passage des Déportés, 2,  
5030 Gembloux, Belgium

C. Fougnes  
Cosucra Groupe Warcoing S.A.,  
Rue de la sucrerie, 1,  
7740 Warcoing, Belgium

J.-C. Lambrechts  
CERTECH, Analytical Sciences—Microscopy,  
Rue Jules Bordet, 1,  
7180 Seneffe, Belgium

product depends on the properties of the feed material.<sup>5</sup> Moreover, it is well established on various well-known products, such as sucrose,<sup>6</sup> trehalose,<sup>7</sup> starch, or dairy products,<sup>8,9</sup> that the state of the matter (amorphous/crystalline) greatly affects the stability or the utilization in many domains, e.g., food industry or pharmaceuticals.

In this paper, the starting material was a semicrystalline sample already spray dried and thus did not completely reflect the process reality. However, in the industry, high degrees of polymerization (DP) inulin are obtained by precipitated fractionation and thus lead to a semicrystalline sample. For this reason, we have used this high DP semicrystalline inulin as a model to investigate the importance of the feed temperature (40–95 °C) and the inlet air temperature of the spray drier (120–230 °C) on the physical and morphological properties of spray-dried inulin. The physical properties estimated were the glass transition temperature ( $T_g$ ) and the crystallinity index, investigated by modulated differential scanning calorimetry (MDSC) and wide angle x-ray scattering (WAXS), respectively. In addition, environmental scanning electron microscopy (ESEM) was used for the surface and particle shape characterization of the powder.

## Materials and methods

### Sample preparation

The inulin sample used was a commercial spray-dried product (Fibruline XL) extracted from chicory roots kindly supplied by Cosucra Groupe Warcoing S.A. (Belgium). Determination of the molecular mass distribution of the sample was done by high performance anion exchange chromatography coupled with pulse amperometric detection (HPAEC-PAD) on a Dionex DX500 chromatographic system operating at 1 ml min<sup>-1</sup>. Twenty-five microliters of a 0.8-g l<sup>-1</sup> solution were injected. Separation of the various chain lengths was achieved on a Dionex PA100 column as described elsewhere.<sup>10</sup> Inulin had an average degree of polymerization number (DP<sub>n</sub>) and weight (DP<sub>w</sub>) of about 23 and 30, respectively.

The dispersions were made to a solid concentration of 20% (w/w) with distilled water at different temperatures (40, 50, 60, 70, 80, 90, and 95 °C). Depending on the feed temperature, the inulin used can be either completely or partially solubilized, which justifies the large temperature range investigated.

### Spray drying

Inulin dispersions were spray dried in a pilot plant scale Anhydro Lab S1 spray drier (Anhydro, Denmark). The liquid was dispersed into a mist in a two-fluid nozzle by means of compressed air. The nozzle was situated in the middle of the drying chamber spraying upwards, whereas the hot air was

simultaneously introduced through an annular opening in the drying chamber ceiling. During the experiments, the liquid feed flow and the nozzle pressure air flow were 2 l h<sup>-1</sup> and 2 bar, respectively. Three inlet air temperatures (compatible with industrial drying conditions of inulins) of 120, 170, and 230 °C were tested, which correspond to outlet air temperature of 65–67, 88–92, and 120–125 °C, respectively. Each inlet air and feed temperature combination was spray dried once.

### Wide angle x-ray scattering

Samples were analyzed in triplicate by WAXS after a procedure previously described elsewhere.<sup>11,12</sup> The apparatus used was a PW3710 Philips Analytical x-ray B.V. with a Ni-filtered CuK $\alpha$  radiation ( $\lambda=1.54178$  Å) generated by an anode device operating at 40 kV and 30 mA in conjunction with a proportional detector. The patterns were recorded with a fixed time of 0.4 s per step of 0.02° in the 4<2 $\theta$ <30° range at 20 °C.

### Modulated differential scanning calorimetry

The thermal properties of powders were examined with a 2920 TA Instruments (New Castle, Delaware, USA) with a Refrigerated Cooling Assesory and modulated capability. The cell was purged with 70 ml min<sup>-1</sup> of dry nitrogen and calibrated for baseline on an empty oven and for temperature using two temperature and enthalpy standards (indium, Tonset: 156.6 °C,  $\Delta H$ : 28.7 J g<sup>-1</sup>; eicosane, Tonset: 36.8 °C,  $\Delta H$ : 247.4 J g<sup>-1</sup>). Specific heat capacity ( $C_p$ ) was calibrated using a sapphire. The empty sample and reference pans were of equal mass to within  $\pm 0.10$  mg. All measurements were made at least in triplicate using nonhermetic aluminum pans.

MDSC curves were obtained over a temperature range of 20–220 °C with a heating rate of 1.5 °C min<sup>-1</sup>, whereas the amplitude and the period of the MDSC were 1.5 °C and 90 s, respectively.

### Environmental scanning electron microscopy

The particle shape and the surface morphology were investigated with an ESEM, XL30 type ESEM-FEG (Philips/FEI) at 20 kV, using wet mode at 2.9 Torr and a working distance of 10.0 mm. The detection system used was a Gaseous Secondary Electron Detector.

## Results and discussion

### Wide angle x-ray scattering

Figure 1a–c shows the WAXS patterns for inulin starting material and its dispersions at 40, 50, 60, 70, 80, 90, and

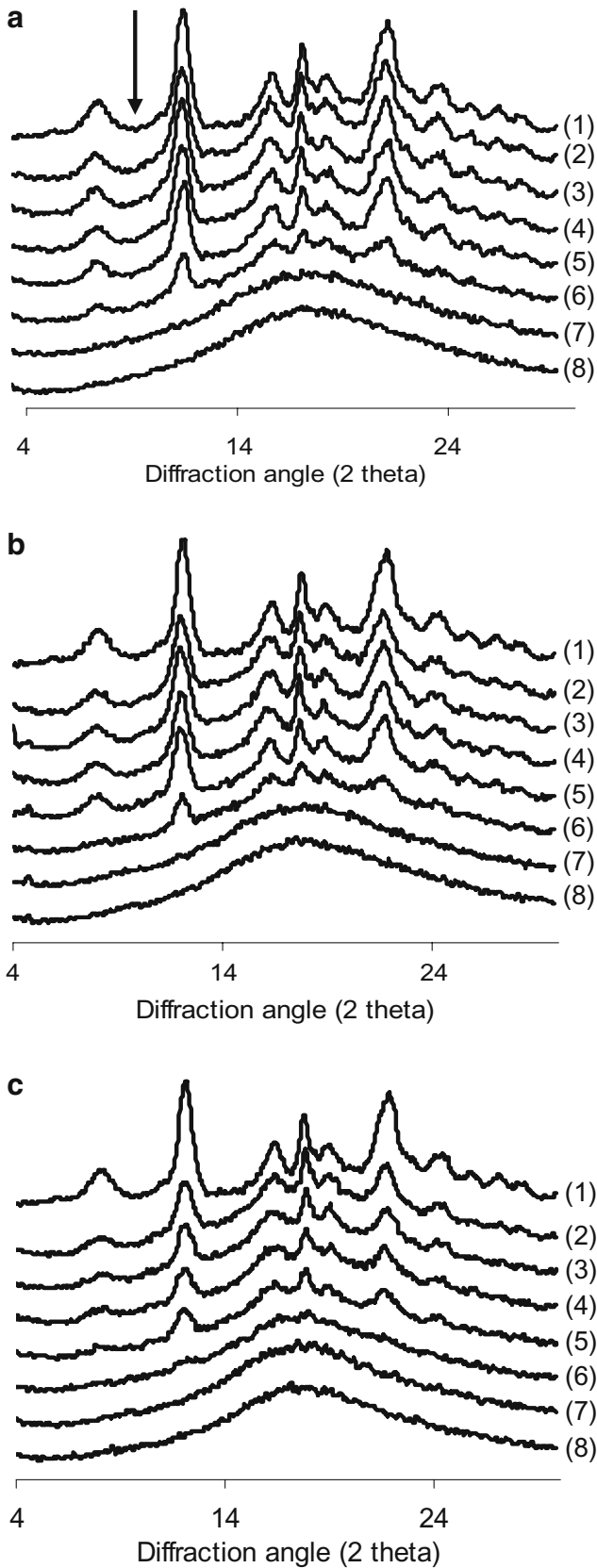


**Fig. 1.** Wide-angle x-ray scattering diffractograms of (1) starting material, inulin dispersion at (2) 40, (3) 50, (4) 60, (5) 70, (6) 80, (7) 90, and (8) 95 °C, spray-dried with an inlet air of **a** 120, **b** 170, or **c** 230 °C. Each diffractogram is the average of three replicates. The arrow points to the absence of the  $2\theta=10.62^\circ$  diffraction peak, confirming the monohydrated crystalline form of our samples.

95 °C, spray dried with an inlet air of 120, 170, or 230 °C. Diffractograms in the  $4^\circ < 2\theta < 30^\circ$  range present either a broad halo pattern or diffraction peaks characteristic of an amorphous or a semicrystalline sample, respectively.<sup>10,12</sup>

The WAXS crystallinity indexes were estimated from the ratio of the integrated intensity of the crystalline peaks to the total integrated intensity of coherent scattering after appropriate baseline subtraction.<sup>13</sup> Each individual diffraction peak was fitted with a Lorentz wave function; whereas a Gaussian function was used for the amorphous halo. For this purpose, the PeakFit™ software was used (PeakFit™ v4.06, AISN Software Inc.). An increase in the feed temperature induced a higher solubilization of inulin and thus increased the amorphous index (100—crystallinity index) as shown in Figure 2.

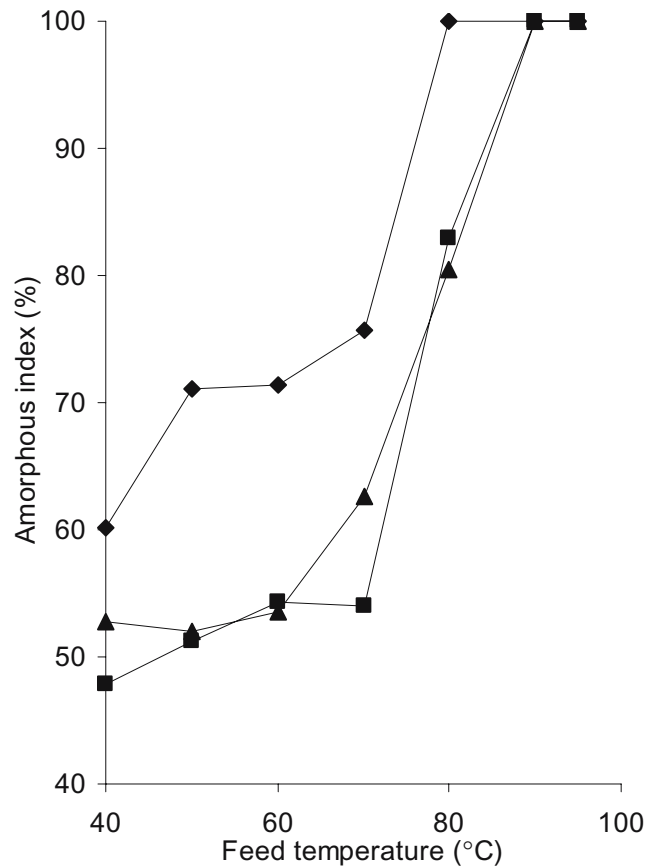


**Fig. 2.** Evolution of the amorphous index (100—crystallinity index) as a function of the dispersion temperature. Samples spray-dried with an inlet air of (■) 120, (▲) 170, or (◆) 230 °C. The reported values are the mean of the crystallinity indexes calculated from the three replicates.

Depending on the feed temperature, the insoluble/soluble ratio of inulin changed (Table 1) as observed after the centrifugation (11,000×g, 10 min) of an aliquot of the dispersed inulin just before the spray drying. This fact is important to underline because it is established that, when a totally soluble product is spray dried, it yields an amorphous powder as the drying time of the droplet is too fast for crystallization to occur. Amorphous inulins were obtained when the insoluble/soluble ratio was equal to zero, corresponding to a feed temperature above 80 °C. Visually, at a temperature between 40 and 80 °C, inulin was either a milky dispersion (up to 70 °C) or a cloudy suspension (80 °C), whereas at higher temperatures (90–95 °C), it was a solution. Thus, amorphous samples were obtained when the inulin suspension feed was transparent, whereas semicrystalline powders were produced by milky or cloudy ones.

As the starting material of the present study was semicrystalline (Figure 1), the nondissolved particles kept this structure during and after drying, leading to a semicrystalline powder. Indeed, optical microscopy under polarized light of inulin feeds has allowed the visualization of dispersed individual crystalline particles (data not shown).

Although the drying of the droplets in a spray drier is a relatively fast phenomenon, we observed that the amorphous content increased at an inlet air temperature of 230 °C (Figure 2). This temperature exceeds the melting point of the semicrystalline inulin (see the MDSC results). Despite the residence time of dried inulin being relatively short in the spray drier, we cannot totally exclude that a small proportion could have been heated at a temperature above the melting point and thus have a higher amorphous content. Indeed, an 80 °C dispersion spray dried with an inlet air temperature of 230 °C yielded a completely amorphous product, whereas at a lower inlet air temperature

(120–170 °C), the feed temperature had to be at 90 °C or above for the same result. This fact is important to emphasize because the method of amorphous production can have an importance on the powder behavior. Surana et al.<sup>7</sup> pointed out that the method of preparation of amorphous trehalose (freeze drying, spray drying, and melt quenching) had an impact on its resistance to crystallization, which is a stability criterion of an amorphous powder. Indeed, it has been found that the structure of amorphous solids is not random, and there is local or short-range order despite the absence of long-range order as in crystals.<sup>14</sup> In our study, the amorphous production was obtained from a concentrated solution although some melting could occur as a result of the high inlet air temperature (230 °C), which is above the melting point. Therefore, the structure of the amorphous material is that of concentrated amorphous solution, which could contain prenucleation centers (i.e., embryonic crystalline organization).

#### Modulated differential scanning calorimetry

In MDSC, the total heat flow between the sample and the reference is described by the following equation<sup>15</sup>:

$$\frac{dQ}{dt} = C_p \cdot b + f(T, t)$$

where  $dQ/dt$  is the resultant heat flow,  $C_p$  is the heat capacity of the sample,  $b$  is the rate of temperature change, and  $f(T, t)$  is the heat flow from kinetic processes. In MDSC, the total heat flow and the two individual components can be distinguished as the heat capacity component ( $C_p \cdot b$ ) or reversing heat flow and kinetic component [ $f(T, t)$ ] or nonreversing heat flow. Because the reversing component is related to the sample heat capacity, a glass transition event is detected in the reversing heat flow. On the other hand,

**Table 1** Chemical composition and insoluble/soluble ratio of water dispersed inulin (20%, w/w) obtained after centrifugation (11,000×g, 10 min) just before spray-drying

	Feed temperature (°C)						
	40	50	60	70	80	90	95
Insoluble/soluble ratio	4.13	0.59	0.56	0.49	0.15	0.00	0.00
Chemical composition							
Supernatant							
DP 1–10	6.4	4.5	4.7	3.9	4.0	3.2	4.0
DP 11–20	36.2	29.2	30.5	25.6	25.7	25.3	26.6
DP 21–30	41.1	40.7	38.9	39.6	39.7	39.8	37.7
DP>30	16.3	25.6	25.9	30.9	30.6	31.7	31.7
DPn	15.3	17.9	17.7	19.2	19.0	20.3	19.4
Pellet							
DP 1–10	2.9	2.7	3.3	2.5	3.6	–	–
DP 11–20	22.2	18.7	20.0	18.2	17.2	–	–
DP 21–30	36.7	36.5	36.4	37.8	35.2	–	–
DP>30	38.2	42.1	40.3	41.5	44.0	–	–
DPn	21.6	22.4	21.4	22.8	21.6	–	–

DP Degree of polymerization,  
DPn degree of polymerization  
in number

processes such as enthalpic relaxation, crystallization, evaporation, or decomposition are resolved into the nonreversing heat flow. For the melting transition, the interpretation is not straightforward. Indeed, melting can occur in the reversing heat flow as well as in the nonreversing heat flow, and the

fraction of melting in both these signals depends on the experimental conditions. As the glass transition is greatly affected by the moisture content, we determined the thermal profiles using open pans, allowing water evaporation and thus measuring the dry T<sub>g</sub>.

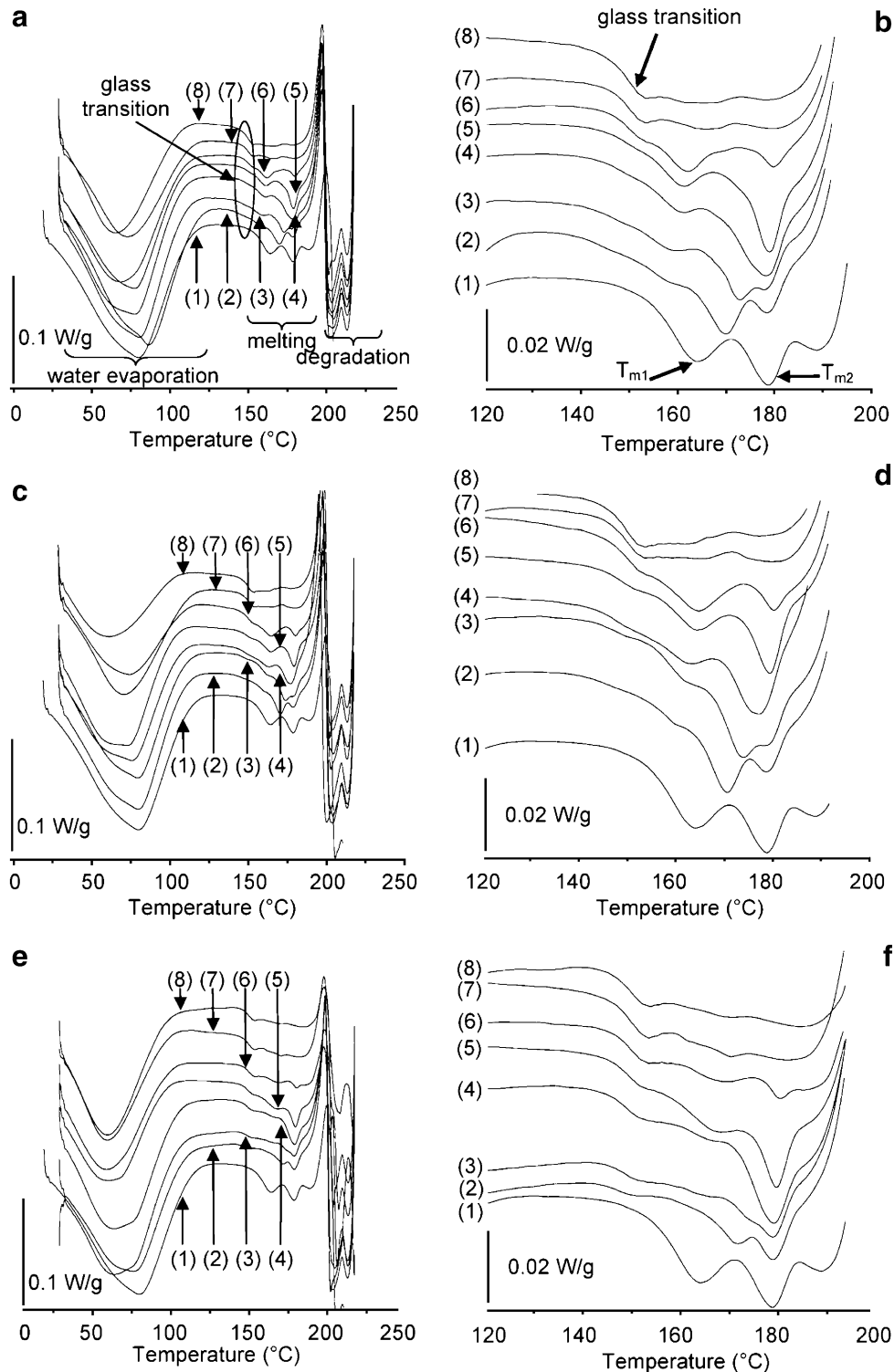


**Fig. 3.** Modulated differential scanning calorimetry thermograms of starting material (1), inulin dispersion at (2) 40, (3) 50, (4) 60, (5) 70, (6) 80, (7) 90, and (8) 95 °C, spray dried with an inlet air of a, b 120; c, d 170; or e, f 230 °C.

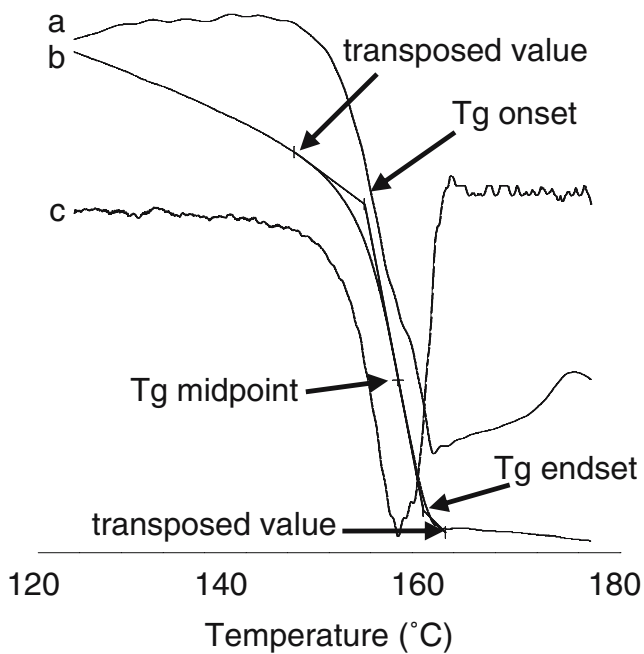


**Fig. 4.** Illustration of the method used to determine the glass transition temperature. (a) total heat flow, (b) reversing heat flow, and (c) temperature derivative of the reversing heat flow signal. The temperature-derived curve of the reversing heat flow component shows a sharp peak at the transition, which gives clear start and end values. These are then transposed on the reversing heat flow signal to determine the onset, midpoint (reported in this study), and endset of the Tg.

MDSC total heat flow curves of inulin dispersions spray dried at an inlet air of 120, 170, and 230 °C are shown in Figure 3a–f. The full temperature range thermograms (Figure 3a, c, and e) allow the visualization of water loss, the glass transition, the melting behavior, and the thermal degradation; whereas Figure 3b, d, and f focus on the thermal events of interest in this study (glass transition and melting). When the products were crystalline, the glass transitions were weak. For this reason, we determined them using the derivative of the reversing component of the total heat flow (Figure 4), which presents a sharp peak at the reversing heat flow jump corresponding to the glass transition. This way, weak glass transitions were observable, although they were only slightly visible in the total heat flow thermograms.

We observed that Tg increased with the feed temperature (Figure 5) and thus with the amorphous content but also when using high inlet air temperature which probably melted some crystals. Such differences in Tg values between a concentrated amorphous solution or a quenched melt have been previously discussed on sucrose by Mathlouthi et al.<sup>16</sup>

Our results are in opposition with those of the synthetic polymer science. Indeed, many authors reported that Tg of the amorphous part increased with the crystallization of the sample (by cold crystallization, annealing, etc.). Usually, the main reason is attributed to the development of a rigid

amorphous phase around crystals and thus a reduction of the mobility of the amorphous region at Tg.<sup>17</sup> In our study, the feed temperature affected the solubility but also the chemical composition of these fractions (Table 1). The average degree of polymerization of the soluble fraction (supernatant), reflecting the molecular weight of the amorphous part of the spray-dried product, increased with the feed temperature. This relationship between molecular weight and the glass transition temperature has been previously described on various amorphous maltodextrins.<sup>18</sup>

In addition to the glass transition determination, MDSC total heat flow curves presented one or two endothermic peaks labeled Tm1 (lower melting peak) and Tm2 (higher melting peak) as indicated by the arrows in Figure 3. Tm1 shifted to a higher temperature as the feed temperature increased, but Tm2 did not shift. The starting material was also characterized by this double endothermic peak. To our knowledge, multiple endotherm behavior has only been reported for semicrystalline synthetic polymers<sup>19–21</sup> and not for oligo- or polysaccharides. In some systems, the origin of the double endothermic peak is attributed to a melting-

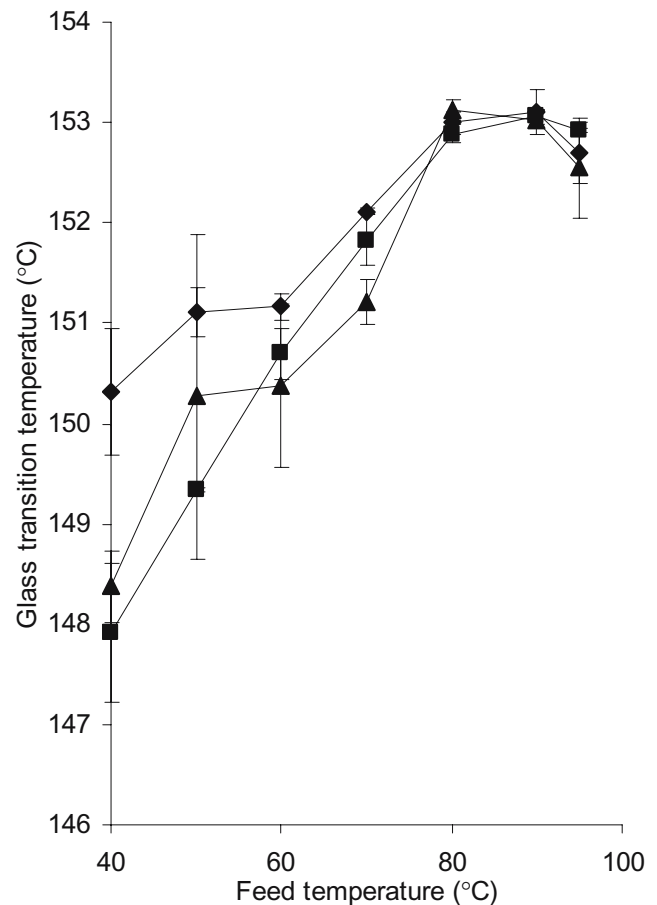


**Fig. 5.** Influence of feed temperature on the dry inulin glass transition temperature. Inulin spray-dried at an inlet air temperature of (■) 120, (▲) 170, or (◆) 230 °C.

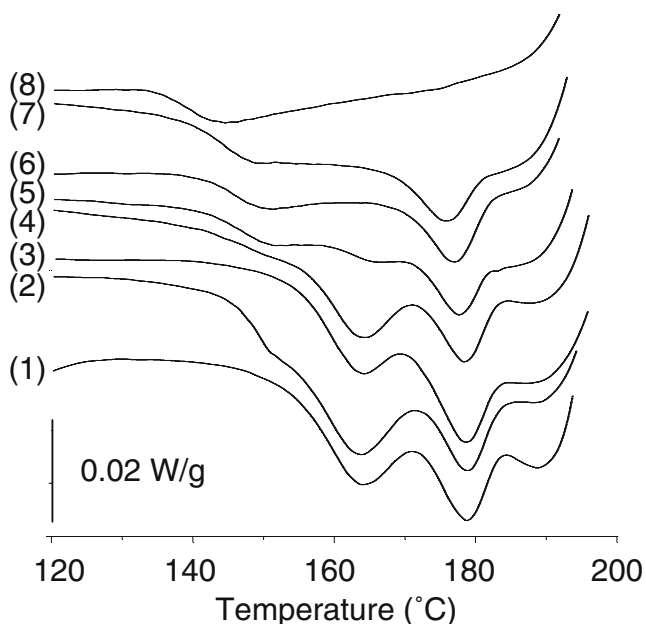


**Fig. 6.** Modulated differential scanning calorimetry thermograms of starting inulin material rescanned after different thermal histories. Starting material (1), first scan up to (2) 140, (3) 156, (4) 164, (5) 171, (6) 176, (7) 180, and (8) 186 °C.

recrystallization-melting phenomena, in which  $T_{m1}$  is attributed to the melting of original crystals, and  $T_{m2}$  is due to the melting of recrystallized material during heating after these crystals have initially melted.<sup>13,22</sup> However, it was not the case in our study. Indeed, a semicrystalline sample (the starting material) was scanned at various heating rates (1, 2.5, 5, 10, 15, and 20 °C min<sup>-1</sup>), and the dual endotherm observed at these different experimental conditions was observed for all heating rates (data not shown). If our system behaved as a melting-recrystallization-melting model, we should have observed a convergence between  $T_{m1}$  and  $T_{m2}$  until only a single endotherm was visible. Indeed, in such a system, at a higher heating rate, the sample passes through the crystallization temperature region so rapidly that there is insufficient time for the melted materials to reorganize into new crystals.<sup>23,24</sup>

Another hypothesis is the existence of dual lamella stacks containing different crystal populations with different melting points.<sup>13</sup> Hébert et al.<sup>25</sup> pointed out two types of crystals during dynamic crystallization from inulin solutions: one resulting from the primary nucleation and thus crystallizing at high temperature and a second one formed by crystallization at lower temperature. Moreover, Hébert<sup>26</sup> presented in his thesis, crystallization of inulin observed by transmission electronic microscopy, confirming a two-phase model consisting of stacks of lamellar crystals separated by amorphous regions. The lamellae formed at low temperature (preponderance of oligofructose) melted at a lower temperature than those formed at high temperature (preponderance of high degree of polymerization

inulin), explaining the existence of two DSC-endotherms. As the starting material of the present study was a fractionated crystallization of native chicory root inulin, we hypothesized that we had two crystal populations, resulting in a dual melting peak obtained by thermal analysis.

Moreover, we heated the starting material to different temperatures (140, 156, 164, 171, 176, 180, and 186 °C) in the MDSC apparatus with the same operating conditions as previously described then immediately quenched them at 20 °C. These temperatures corresponded to different positions on the double endotherm (before, during, and after each transition), and the MDSC rescan of these samples is presented in Figure 6.

Each endotherm was visible as long as the previous heating did not exceed the end of the concerned transition. When a crystal population was melted, the sample could not recrystallize during the cooling and the rescan because the crystal structure needed water in its unit cell lattice.<sup>27–29</sup> Therefore, the endotherms observed were an irreversible phenomenon and thus not only corresponded to the melting of the crystals but also to the release of the water of crystallization. Indeed, it is established that depending on the hydration conditions, there are two crystalline inulin allomorphs: a monohydrated form and a hemihydrated form. The difference between these unit cells is an additional diffraction peak at  $2\theta=10.62^\circ$  for the hemihydrated form. However, in all WAXS experiments, the inulin diffractograms obtained in this study were only characteristic of the monohydrated form.

Moreover, a linear relationship was found between the crystallinity index and enthalpy (melting peak area) if the

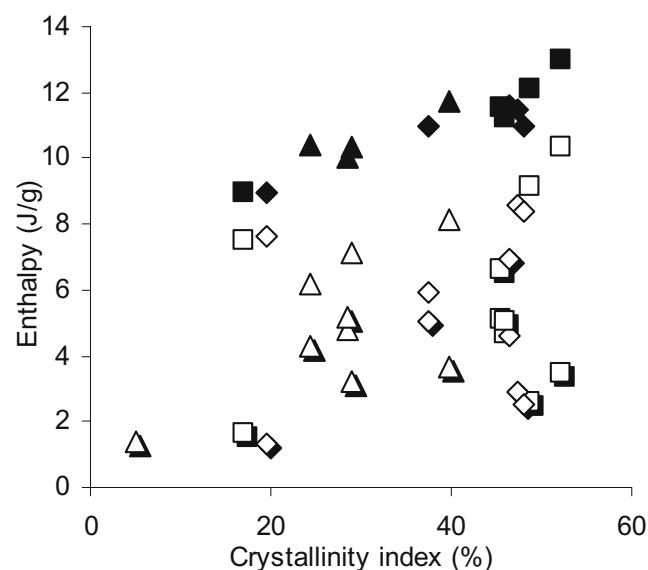
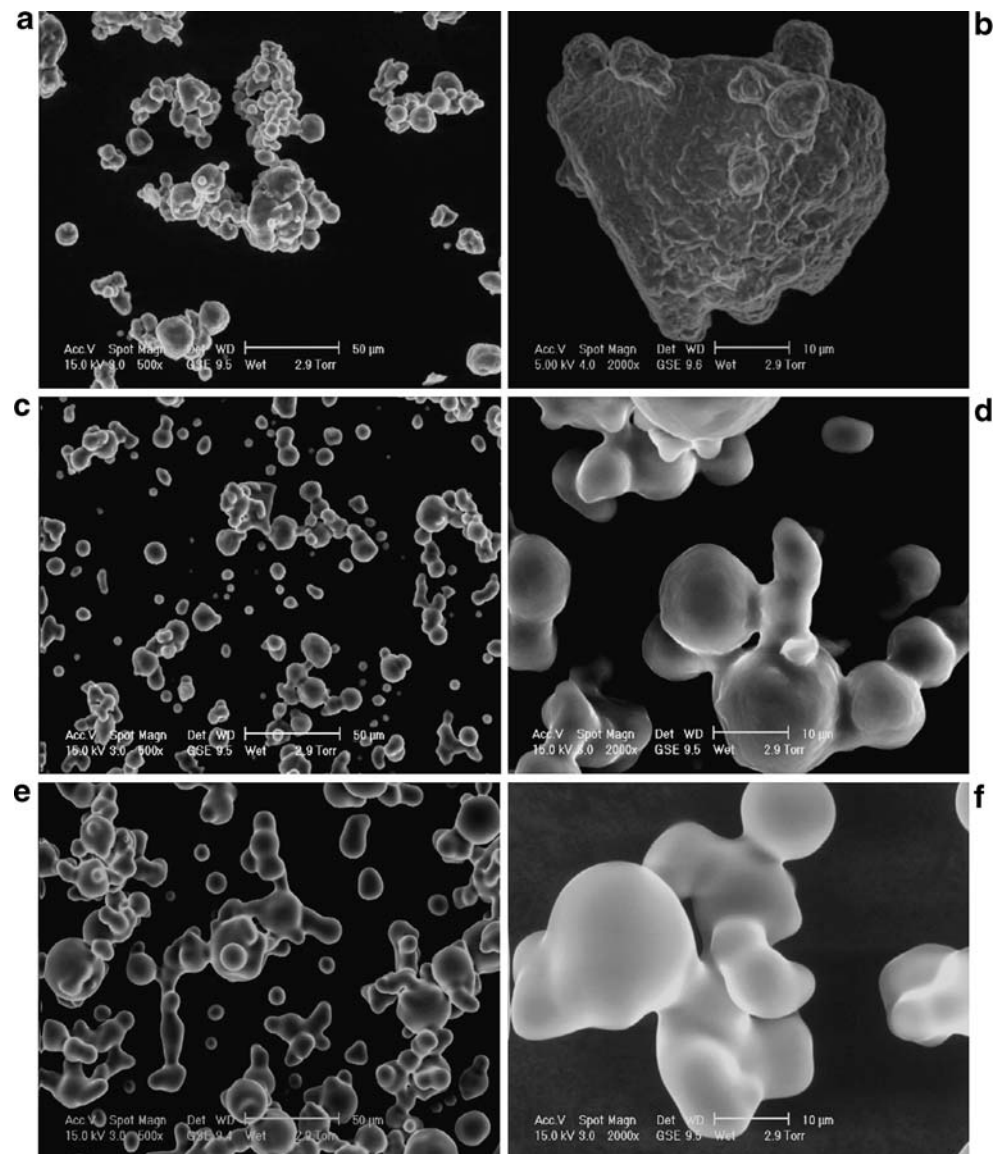


**Fig. 7.** Relationship between enthalpy and crystallinity index of inulin dispersion spray-dried with an inlet air of (square) 120, (lozenge) 170, or (triangle) 230 °C. Hm1 (open symbols), Hm2 (shaded symbols), and Htot (closed symbols) represent the enthalpy of the first, the second, and the sum of the melting peaks, respectively.

**Fig. 8.** ESEM micrographs of spray-dried inulin illustrating the variation in particle shape and surface roughness when produced from different dispersion temperatures at an inlet air temperature of 120 °C. **a** and **b**:  $T_{\text{feed}}=40$  °C, **c** and **d**:  $T_{\text{feed}}=70$  °C, **e** and **f**:  $T_{\text{feed}}=95$  °C. Scale bar for **a**, **c**, and **e**: 50  $\mu\text{m}$ ; scale bar for **b**, **d**, and **f**: 10  $\mu\text{m}$ .



sum of the two endothermic peaks was taken into account (Figure 7).

Individual enthalpy (open and shaded symbols for Hm1 and Hm2, respectively) cannot be correlated with the crystallinity index, arguing the fact that both melting peaks were related to the crystallinity of the sample.

#### Morphological characterization

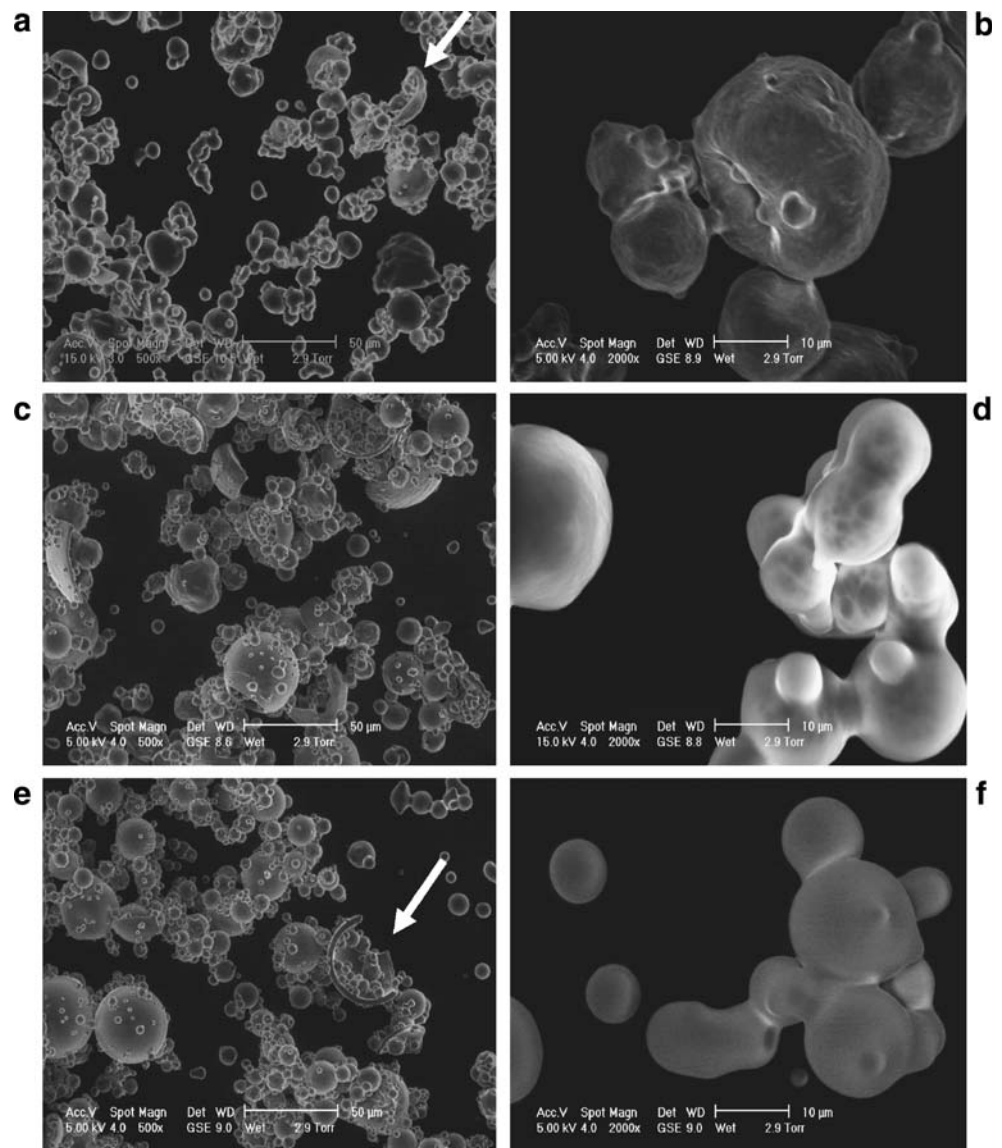
Figures 8–9 illustrate ESEM micrographs of inulin dispersed at 40, 70, and 95 °C and spray dried with an inlet air temperature of 120 or 230 °C. The particles presented various shapes with a rough or smooth surface. The main differences between particle morphologies were observed for the various feed temperatures and were probably due to a difference in the melting of crystals present in the dispersion. At a temperature between 40 and 80 °C, inulin

was either a milky dispersion (up to 70 °C) or a cloudy suspension (80 °C), whereas at higher temperatures (90–95 °C), it was a transparent solution.

Other studies that investigated spray drying from solution rather than suspensions also noted the formation of smooth spherical particles.<sup>30,31</sup> Increasing the temperature of the feed led to a smoother powder surface probably because of the spray drying of a solution rather than a dispersion. The drying of a dispersion containing undissolved solid particles ( $T_{\text{feed}} < 80$  °C) led to powders with rough surfaces. During the atomization of the feed in the spray drying chamber, the undissolved solid particles can be fused together probably by the presence of solubilized inulin on their surface. Indeed, the rapid evaporation of a solution leads to an amorphous sample characterized by a glass transition temperature. If the temperature of the powder is above  $T_g$ , the particles become sticky and can



**Fig. 9.** Environmental Scanning Electron Microscopy (ESEM) micrographs of spray-dried inulin, illustrating the variation in particle shape and surface roughness when produced from different dispersion temperatures at an inlet air temperature of 230 °C. **a** and **b**:  $T_{\text{feed}}=40$  °C, **c** and **d**:  $T_{\text{feed}}=70$  °C, **e** and **f**:  $T_{\text{feed}}=95$  °C. Scale bar for **a**, **c**, and **e**: 50  $\mu\text{m}$ ; scale bar for **b**, **d**, and **f**: 10  $\mu\text{m}$ .



be joined together. This transition is dependent of the moisture content but also of the molecular weight of the amorphous sample. The bridges between particles is called agglomeration and can be considered as a size enlargement process for powders, where small particles combine to form relatively large permanent masses in which the original particles are still identifiable. It is often required in the food industry to produce quick dissolving or dispersing powders in solvents like water or milk, without the formation of lumps. The origin of this agglomeration may result from two different processes<sup>32,33</sup>: a primary agglomeration caused by collision of primary spray particles with each other and a secondary agglomeration caused by collision of primary spray particles with fines (dry particles). As the spray drier used in the present study had no fines recycler, the agglomerated particles were mainly due to a primary agglomeration. However, we cannot totally exclude a

random unprovoked collision in the spray drier of dry and moist particles caused by the swirl flow.

This agglomeration also occurred at a high feed temperature, where single droplets from solubilized feed were joined together. The viscosity of the droplet and thus the feed temperature can influence the size and shape of individual particles. Indeed, Bain et al.<sup>34</sup> considered how the particle size of spray-dried powders might be influenced by the viscosity of the formulation, and other works have commented that viscosity of the spray-drying formulation is one of several crucial factors that determine the morphology of resultant particles.<sup>35</sup> Moreover, a change in the viscosity of the feed might influence the behavior of the solution at the spray-drier nozzle and hence affect the size of the droplets produced.<sup>31</sup>

At an inlet air temperature of 120 and 170 °C, the solid particles were intact; whereas at 230 °C, the surfaces were

damaged. During drying, internal heat transport (conduction) takes place quickly in comparison with the internal mass transport (diffusion).<sup>33</sup> For this reason, a skin is formed on the outer surface of the spray droplets. The internal mass transport is often the rate-limiting factor, and as a consequence, moisture gradients are formed inside the powder particles.<sup>33</sup> This moisture might provide an overpressure inside the particle and lead to the rupture of the outer surface. Thus, the external transport phenomena (from particle surface to surrounding air) and the internal transport phenomena (within particles) both play a role during the drying process<sup>33</sup> and are important to the final shape of the powder.

## Conclusions

The feed temperature and the inlet temperature were found to have significant effects on the physical and morphological properties of spray-dried inulin. An increase in the feed temperature or, to a lesser extent, the inlet air temperature resulted in an increase of the amorphous content in the spray-dried products. By selecting appropriate feed or inlet air temperatures, we were able to produce spray-dried inulin with the desired physical properties. Such properties are of crucial importance to the hygroscopic properties and thus can affect the stability of the product in many domains like food technology or pharmaceuticals. Stability of a powder is directly linked to its glass transition temperature. Indeed, when  $T_g$  is lower than the storage temperature, stability problems occurred, such as crystallization or caking.<sup>12</sup> As it is well established that amorphous products are more hygroscopic than their crystalline counterparts, this could inevitably have an impact on their behavior during storage. For this reason, the impact of storage conditions on both stability and product quality of amorphous and semicrystalline inulin will be evaluated and discussed in further studies.

**Acknowledgment** We thank Mrs. Lynn Doran for technical assistance, Mrs. Bernadette Norberg and Prof. Johan Wouters from the 'Department of Structural Biological Chemistry' of the 'Facultés universitaires Notre Dame de la Paix' (Namur, Belgium) for the use of the WAXS, and Mrs. Anne-Sophie Quique from Cosucra Groupe Warcoing S.A. for the HPAEC-PAD experiments.

Financial support was provided for this study by the Walloon Region of Belgium (DGTRE) and Cosucra Groupe Warcoing S.A.

## References

- C. Blecker, C. Fougnyes, J.C. Van Herck, J.P. Chevalier and M. Paquot, *J Agric Food Chem* **50**, 1602–1607 (2002).
- M.B. Roberfroid and N.M. Delzenne, *Annu Rev Nutr* **18**, 117–143 (1998).
- C. Blecker, J.P. Chevalier, J.C. Van Herck, C. Fougnyes, C. Deroanne and M. Paquot, *Recent Research Developments in Agricultural & Food Chemistry* **5**, 125–131 (2001).
- D.E. Oakley, *Chem Eng Prog* **93**, 48–54 (1997).
- O.C. Chidavaenzi, G. Buckton, F. Koosha and R. Pathak, *Int J Pharm* **159**, 67–74 (1997).
- M. Sugimoto, T. Maejima, S. Narisawa, K. Matsubara and H. Yoshino, *Int J Pharm* **296**, 64–72 (2005).
- R. Surana, A. Pyne and R. Suryanarayanan, *Pharm Res* **21**, 1167–1176 (2004).
- R. Parker and S.G. Ring, *J Cereal Sci* **34**, 1–17 (2001).
- J.J. Fitzpatrick, K. Barry, P.S.M. Cerqueira, T. Iqbal, J. O'Neill and Y.H. Roos, *Int Dairy J* **17**, 383–392 (2007).
- S.N. Ronkart, M. Paquot, C. Fougnyes, C. Deroanne, J.C. Van Herck and C. Blecker, *Talanta* **70**, 1006–1010 (2006).
- C. Blecker, J.P. Chevalier, C. Fougnyes, J.C. Van Herck, C. Deroanne C. and M. Paquot, *J Therm Anal Cal* **71**, 215–224 (2003).
- S. Ronkart, C. Blecker, C. Fougnyes, J.C. Van Herck, J. Wouters and M. Paquot, *Carbohydr Polym* **63**, 210–217 (2006).
- H. Xu, B. Seyhan Ince and P. Cebe, *J Polym Sci Pol Phys* **41**, 3026–3036 (2003).
- E.Y. Shalaev and G. Zografi, The concept of structure in amorphous solids from the perspective of the pharmaceutical sciences. In: *Progress in Amorphous Food and Pharmaceutical Systems*, edited by H. Levine (Royal Society of Chemistry, Cambridge, UK 2002), pp. 11–30.
- E. Verdonck, K. Schaap, L.C. Thomas, *Int J Pharm* **192**, 3–20 (1999).
- M. Mathlouthi, A.L. Cholli, and J.L. Koenig, *Carbohydr Res* **147**, 1–9 (1986).
- J.F. Mano, J.L. Gómez Ribelles, N.M. Alves and M. Salmerón Sanchez, *Polymer* **46**, 8258–8265 (2005).
- Y. Roos and M. Karel, *Biotechnol Prog* **7**, 49–53 (1991).
- S.Y. Hobbs and C.F. Pratt, *Polymer* **16**, 462–465 (1975).
- C. Fougnyes, M. Dosière, M.H.J. Koch and J. Roovers, *Macromolecules* **31**, 6266–6274 (1998).
- E.M. Woo, Y.S. Sun and C.P. Yang, *Prog Polym Sci* **26**, 945–983 (2001).
- J. Plans, W.J. MacKnight and F.E. Karasz, *Macromolecules* **17**, 810–814 (1984).
- T. Liu, *Eur Polym J* **39**, 1311–1317 (2003).
- P. Sriramoan, N. Dangseeun and P. Supaphol, *Eur. Polym. J.* **40**, 599–608 (2004).
- C.L.M. Hébert, J.A. Delcour, M.H.J. Koch, K. Booten, R. Kleppinger, N. Mischenko and H. Reynaers, *Carbohydr Res* **310**, 65–75 (1998).
- Hébert C, *Crystallisation, melting and gel formation of concentrated inulin-water systems*. PhD thesis (K.U. Leuven, Belgium 2002).
- R.H. Marchessault, T. Bleha, Y. Deslandes and J.F. Revol, *Can J Chem* **58**, 2415–2422 (1980).
- I. André, J.L. Putaux, H. Chanzy, F.R. Taravel, J.W. Timmermans and D. de Wit, *Int J Biol Macromol* **18**, 195–204 (1996a).
- I. André, K. Mazeau, I. Tvaroska, J.L. Putaux, W.T. Winter, F.R. Taravel and H. Chanzy, *Macromolecules* **29**, 4626–4635 (1996b).
- D.O. Corrigan, A.M. Healy and O.I. Corrigan, *Int J Pharm* **262**, 125–137 (2003).
- N.R. Rabbani and P.C. Seville, *J Control Release* **110**, 130–140 (2005).
- B.H. Graham, *Food Austr* **49**, 184–185 (1997).
- R.E.M. Verdurmen, P. Menn, J. Ritzert et al., *Dry Technol* **22**, 1403–1461 (2004).
- D.F. Bain, D.L. Munday and A. Smith, *J Microencapsul* **16**, 453–474 (1999).
- F. Iskandar, L. Gradon and K. Okuyama, *J Colloid Interf Sci* **265**, 296–303 (2003).